euspen's 25th International Conference & Exhibition, Zaragoza, ES, June 2025
www.euspen.eu

Lateral dimension and mapping distortion calibration method for wavefront interferometers utilizing a calibration plate

YUNFENG MAO[1, 2, 3], SHUAI XUE[1, 2, 3*], ZUBO HU[1, 2, 3], ANTONG HUANG[1, 2, 3], AND XIAOQIANG PENG[1, 2, 3]

[1] *National Key Laboratory of Equipment State Sensing and Smart Support ,College of Intelligence Science and Technology, National University of Defense Technology, Changsha, Hunan, 410073, China*
[2] *Hunan Key Laboratory of Ultra-Precision Machining Technology, Changsha, Hunan, 410073, China*
[3] *Hunan Institute of Advanced Technology, Changsha, Hunan, 410073, China*

**shuaixue1990@163.com*

Abstract

The development of synchrotron radiation and free-electron laser facilities requires X-ray mirrors with form accuracy better than 50 nrad Root-Mean-Square (RMS) and 2 nm Peak-to-Valley (PV). For obtaining the form error of X-ray mirrors and directing the deterministic figuring process, wavefront interferometry is commonly utilized. For calibrating the reference form error of the wavefront interferometers, absolute test techniques are utilized. The prevailing shear-shift kind of absolute test methods demand translating the test surface with distance equalling multiples of integer of dimension of pixels. Moreover, the mapping distortion of the CCD coordinates with the test surface coordinates also introduces test error. This paper presents a method for lateral dimension calibration and map distortion evaluation of wavefront interferometers that uses a calibration plate fabricated by micro and nano craft. Circular dots with precision dimensions and locations was printed on the plate. By testing the plate with the wavefront interferometer and processing the test result with image processing techniques, the lateral dimension and map distortion of the interferometer can be calibrated. A 4-inch wavefront interferometer is calibrated utilizing the proposed method. The repeatability of the calibration results was analysed. Using the calibration result, the shear-shift absolute test method can be further developed to enhance the test accuracy to meet the on-going accuracy requirements posed by X-ray mirrors.

Wavefront interferometry, lateral dimension calibration, distortion evaluation, absolute test

1. Introduction

Next-generation synchrotron radiation sources and free electron laser facilities require X-ray mirror surface figure accuracy exceeding 50 nrad RMS and 2 nm PV[1–4]. To obtain surface height data for guiding deterministic polishing, wavefront interferometry is typically employed[5,6]. However, the accuracy of wavefront interferometry is influenced by several factors, including the calibration of lateral dimensions and mapping distortions.

As a classic dual-wave interferometric system, the absolute measurement accuracy of wavefront interferometers fundamentally relies on the manufacturing precision of reference flats. To address reference surface errors, shear translation-based absolute measurement methods are commonly employed[7–10]. This technique necessitates integer-pixel-level shear displacements in CCD coordinates, and any inaccuracies in evaluating single-pixel dimensions can compromise the overall measurement accuracy. Additionally, as an interferometric imaging system, it is subject to inherent systematic errors caused by optical aberrations,which can violate common-path conditions and induce retrace errors [11]. Therefore, to meet pixel-level shear displacement requirements and eliminate lateral distortion in the measured surface data, enhanced calibration of CCD pixel dimensions and precise evaluation of lateral distortion are essential for achieving superior absolute measurement accuracy.

Conventional lateral dimension calibration use optical imaging of precision gauge blocks to determine pixel dimensions through a comparative analysis of measured pixel dimensions and nominal physical sizes. For full-aperture lateral distortion characterization, traditional methods utilize high-precision array calibration plates, assessing distortion across the entire aperture by analyzing positional deviations among array patterns [12].

However, lateral distortion typically manifests as a non-uniform distribution of pixel dimensions across the full aperture. Conventional calibration methods cannot address these full-aperture dimensional variations, resulting in significant calibration errors. Furthermore, CCD-captured grayscale images, which are limited to 256 intensity levels, inherently restrict edge detection accuracy and hinder sub-pixel-level dimensional extraction.

To address these limitations, this study proposes a calibration methodology that combines lateral dimension measurement with distortion characterization using precision calibration plates. Vy leveraging the inherent surface measurement capabilities of wavefront interferometers, we convert the measured surface height data of the calibration plates into grayscale image representations. The subsequent implementation of machine vision algorithms for edge detection and feature extraction of least squares[13–15] enables the reconstruction of feature distribution grids on the calibration plates. This approach enhanceslateral dimension calibration and distortion evaluation for pixel-level measurement techniques, such as dual-shear translation methods.

2. Methods

The calibration methodology for lateral scale and mapping distortion in wavefront interferometry using calibration plates consists of four key procedural stages, as illustrated in Figure 1:

1. **Surface Topography Acquisition**: The surface topography of the calibration plate is measured using the wavefront interferometer.
2. **Grayscale Image Conversion**: The acquired height data is transformed into an enhanced-contrast grayscale image representation of the surface morphology.
3. **Feature Point Extraction**: Edge detection and feature extraction algorithms are systematically applied to identify characteristic marker arrays, generating precise feature point coordinate datasets.
4. **Dimensional and Distortion Analysis**: Lateral dimension calibration and mapping distortion evaluation are performed through computational analysis of the extracted feature point coordinate arrays.

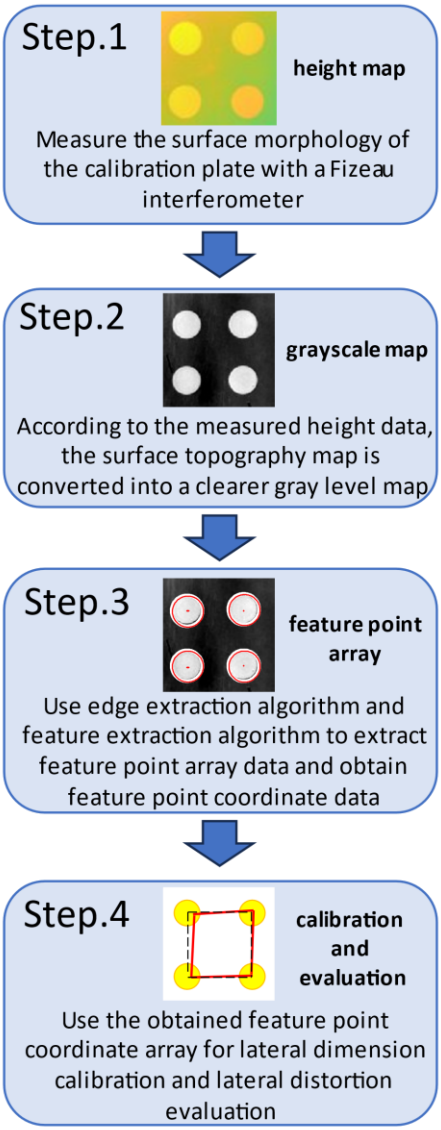

Figure 1. The steps of lateral dimension and mapping distortion calibration method for wavefront interferometers utilizing a calibration plate.

2.1 Material and instrument

The experimental setup utilized a 4-inch Zygo Verifire Fizeau interferometer equipped with a 1200×1200 pixels CCD. To enable full-aperture distortion characterization, a calibration plate measuring 152.4x152.4 mm (6 inches) and 6.35 mm thick was employed(see Figure 2). This calibration plate features a fused quartz substrate that supports a 15×15 array of solid chromium-plated dots, each with a height of 100 nm. The dots have diameters of 4 mm ±100 nm and are spaced 8 mm ±100 nm apart. To facilitate the measurement of surface topography on the chromium-plated surface, the opposing side of the calibration plate was coated with a diffuse reflective layer.

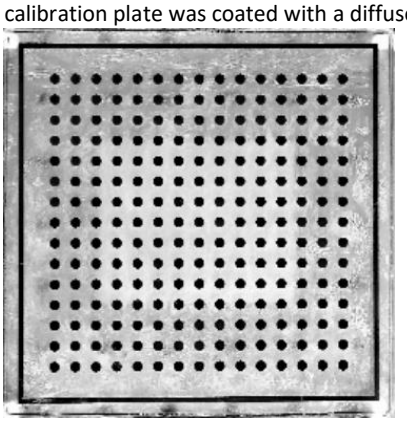

Figure 2. High precision 152.4x152.4mm calibration plate

2.2 Extraction of feature points from the calibration plate

The surface topography of the calibration plate, measured using the 4-inch Fizeau interferometer, is shown in Figure 3(a), where the chromium-plated dots are partially resolved. However, residual tilt artifacts, resulting from incomplete nulling during the measurement, introduced significant low-order surface deviations that prevented a direct grayscale conversion from the raw height data. To address this issue, a fourth-order polynomial surface was optimally fitted and subtracted from the original topography to eliminate low-order form errors.

The processed height data was partitioned into 256 discrete intervals corresponding to grayscale values, resulting in the converted grayscale image shown in Figure 3(b). A Sobel edge detection algorithm was then systematically applied to extract the edges of the dots, followed by least-squares circle fitting to determine the centroid coordinates for each dot cluster. This procedure yielded the characteristic feature point distribution presented in Figure 3(c).

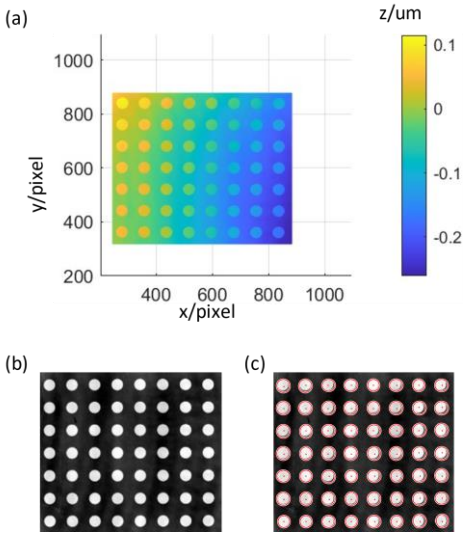

Figure 3. The extraction process of the feature points of the calibration plate (a) calibration plate surface topography (b) calibration plate grayscale map (c) feature extraction diagram of the calibration plate

2.3 Lateral dimension calibration and mapping distortion evaluation

The feature point (dot centroid) dataset obtained from Section 2.2 allows for the establishment of a characteristic grid structure. By calculating the distances between adjacent markers (in pixels) and applying spatial averaging, we derive a mean inter-dot distance, denoted as *d*.Using the physical inter-dot distance ,*D,* of the calibration plate, the lateral scale of the interferometer is determined using Equation (1):

$$pix = D / d \quad (1)$$

where *pix* represents the interferometer's lateral scale (unit: mm/pixel), *D* denotes the physical inter-dot spacing of the calibration plate (unit: mm), and *d* corresponds to the averaged extracted distance between adjacent feature points (unit: pixel).

Using the calibrated lateral scale, a reference feature point grid can be constructed. By calculating the positional deviations between each measured feature point and its corresponding reference grid node, a mapping distortion profile is generated. Systematic analysis of this distortion map allows for a quantitative characterization of distortion across the measurement domain.

3. Experimental Results

3.1 Masked rectangular aperture evaluation

The rectangular measurement domain was systematically analyzed, resulting in distortion grid maps and spatial distortion profiles with 10× magnification of inherent deformations, as shown in Figures 4(a) and 4(b).

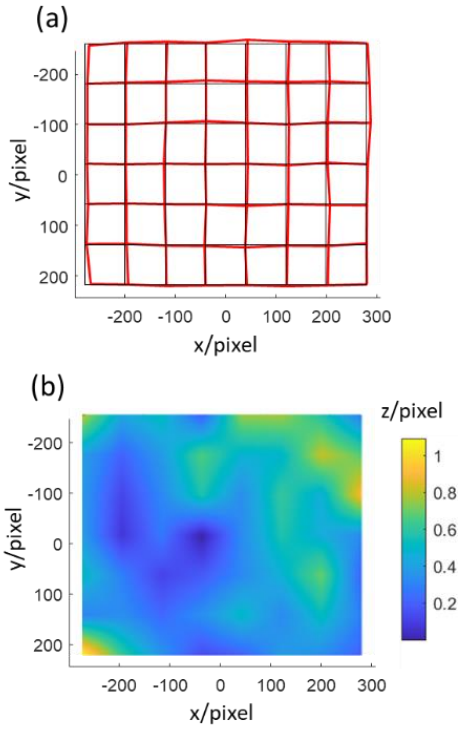

Figure 4. Masked rectangular aperture evaluation (a) Distorted grid diagram (b) Distortion profile

The lateral scale calculated using Equation (1) yielded a value of **0.100404 mm**. As shown in Figure 4(b), the maximum distortion reached **1.089 pixels** (equivalent to **0.109340 mm**). Visual inspection indicates that significant distortion primarily occurs in the peripheral regions of the measurement domain.

3.2 Full aperture evaluation

Full aperture distortion characterization of the calibration plate was conducted, resulting in distortion grid maps and spatial distortion profiles with **10× magnification** of inherent deformations, as illustrated in Figures 5(a) and 5(b).

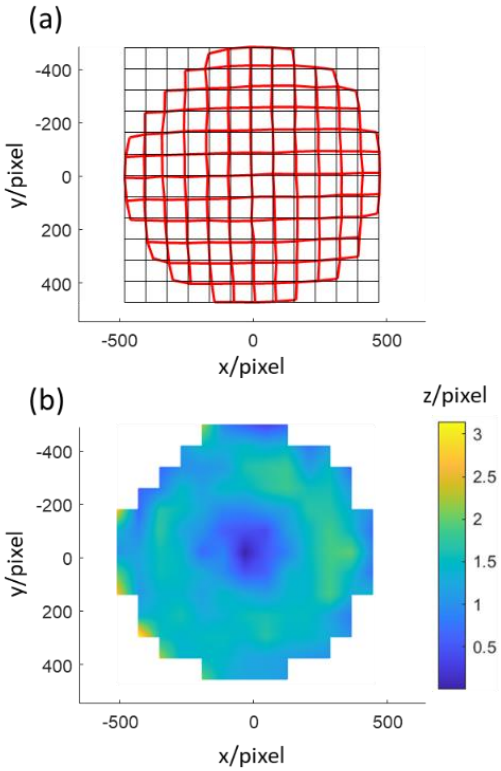

Figure 5. Full aperture evaluation (a) Distorted grid diagram (b) Distortion profile

The calculated full-aperture lateral scale was determined to be **0.100865 mm**. Figure 5(b) shows a maximum distortion of **3.033 pixels**, which significantly exceeds the results from Section 3.1. This discrepancy likely arises from the non-ideal circular profiles of peripheral dots under full-aperture conditions (see Figure 6). The reduced number of data points available for least-squares computation, copared to complete circles, introduces amplified calculation errors. Systematic analysis reveals a strong positive correlation between the magnitude of lateral distortion and proximity to the aperture boundaries.

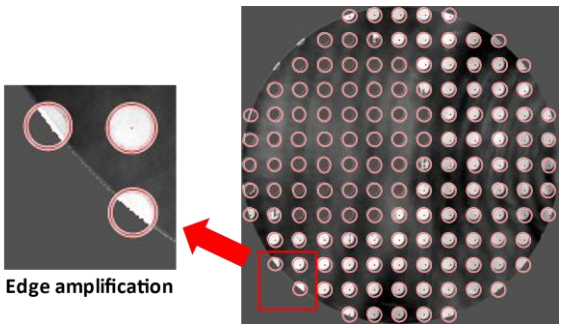

Figure 6. When extracting feature points, the full aperture edge dot situation

4. Discussion

1. Experimental results show consistent maximum distortion localization in the peripheral regions for both rectangular sub-aperture and full-aperture evaluations

(Figure 4-5). This spatial correlation likely arises from aberration accumulation effects (e.g., field curvature or distortion aberrations), that are inherent to the interferometer's optical system and become more pronounced at off-axis positions. Additionally, the compromised edge integrity of peripheral calibration dots (Figure 6) reduces the number of available data points for circle fitting, thereby increasing computational uncertainties.

2. The lateral scale calibration resulted in **0.100404 mm** for localized sub-apertures and **0.100865 mm** for full aperture measurements. Spatial averaging ensured that calibration repeatability was maintained at sub-micron levels.
3. Our methodology utilizes chromium-dot array calibration plates along with Sobel edge detection and least-squares fitting algorithms to achieve superior feature localization accuracy at the sub-pixel level. In compared to conventional edge extraction from native grayscale images, our height-data-to-grayscale conversion technique enhances feature contrast while reducing noise interference.
4. Critical attention must be directed toward systematic error contributions arising from **calibration plate dot fabrication tolerances (±100 nm)** and **residual low-order surface deviations associated with imperfect interferometric nulling**. These inherent limitations can be mitigated through the strategic optimization of calibration plate manufacturing protocols or the implementation of advanced self-calibration algorithms[16], thereby enabling subsequent improvements in metrological precision.

5. Conclusion

This study presents a novel calibration methodology for lateral scale characterization and mapping distortion evaluation in wavefront interferometry using precision calibration plates. By converting calibration plate surface topography data into grayscale imagery integrated with machine vision algorithms, we achieve full-aperture pixel-level lateral dimension calibration and distortion distribution analysis. Experimental calibration results demonstrate a lateral scale of **0.100404 mm** within a masked rectangular aperture and **0.100865 mm** across the full aperture for the 4-inch Zygo Verifire interferometer's CCD system. Furthermore, systematic analysis of distortion profiles reveals a progressive intensification of distortion magnitude toward the peripheral regions, exhibiting a strong spatial correlation with proximity to aperture boundaries. Additionally, experimental results demonstrate the method's capability to effectively identify peripheral distortion patterns while quantifying their spatial characteristics with sub-pixel accuracy. Compared to conventional approaches, our methodology resolves the critical challenge of full-aperture nonlinear distortion characterization, providing essential parametric support for enhancing shear-scanning absolute detection techniques. This advancement holds significant potential for improving X-ray mirror surface metrology precision, ultimately meeting the ultra-stringent specifications required by next-generation synchrotron radiation sources and free electron laser facilities. Future research will focus on optimizing calibration plate fabrication processes and algorithmic robustness to extend the applicability of this methodology to complex optical system characterization.

References

[1] Yumoto H, Mimura H, Koyama T, Matsuyama S, Tono K, Togashi T, Inubushi Y, Sato T, Tanaka T, Kimura T, Yokoyama H, Kim J, Sano Y, Hachisu Y, Yabashi M, Ohashi H, Ohmori H, Ishikawa T and Yamauchi K 2013 *Nature Photon.* **7**(1) 43–47

[2] Siewert F, Buchheim J, Boutet S, Williams G J, Montanez P A, Krzywinski J and Signorato R 2012 *Opt. Express* **20**(4) 4525

[3] Matsuyama S, Wakioka T, Kidani N, Kimura T, Mimura H, Sano Y, Nishino Y, Yabashi M, Tamasaku K, Ishikawa T and Yamauchi K 2010 *Opt. Lett.* **35**(21) 3583

[4] Schmoldt A, Benthe H F and Haberland G 1975 *Biochem Pharmacol* **24**(17) 1639–41

[5] Dai Y, Zhou L, Xie X, Jiao C and Li S 2008 *Acta. Opt. Sinica.* (6) 1131–35

[6] Dai Y, Shi F, Peng X and Song C 2010 *Acta. Opt. Sinica.* **30**(1) 198–205

[7] Ma J, Pruss C, Zhu R, Gao Z, Yuan C and Osten W 2011 *Opt. Lett.* **36**(11) 2005

[8] Morin F and Bouillet S 2007 in W. Osten, C. Gorecki and E. L. *Novak eds.* p. 66164G

[9] Zhai D, Chen S, Shi F and Yin Z 2017 *Opt. Commun.* **402** 453–61

[10] Zhai D, Chen S, Xue S and Yin Z 2016 *Appl. Opt.* **55**(28) 8063

[11] Kreischer C B 2013 in J. L. Bentley and M. *Pfaff eds.* p. 88840X

[12] Henning A, Giusca C, Forbes A, Smith I, Leach R, Coupland J and Mandal R 2013 *CIRP Ann.* **62**(1) 547–50

[13] Qiao X, Chen X, Ekberg P, Ding G, Cai X, Wei J and Wu J 2019 *Meas. Sci. Technol.* **30**(12) 125015

[14] Qiao X, Ding G, Chen X and Cai P 2021 *IEEE Trans. Instrum. Meas.* **70** 1–8

[15] Qiao X, Ding G, Chen X, Cai P and Shao L 2022 *IEEE Trans. Instrum. Meas.* **71** 1–9

[16] Evans C J, Hocken R J and Estler W T 1996 *CIRP Ann.* **45**(2) 617–34